Available online at www.sciencedirect.com

SCIENCE DIRECT®

Earth and Planetary Science Letters 229 (2004) 141–154

EPSL

www.elsevier.com/locate/epsl

Anaerobic methane oxidation and the formation of dolomite

T.S. Moore[a,*], R.W. Murray[b,1], A.C. Kurtz[c,2], D.P. Schrag[d,3]

[a]*Department of Earth Sciences, Boston University, Boston, MA 02215, United States*
[b]*Department of Earth Sciences, Boston University, 685 Commonwealth Ave., Boston, MA 02215, United States*
[c]*Department of Earth Sciences, Boston University, 695 Commonwealth Ave., Boston, MA 02215, United States*
[d]*Department of Earth and Planetary Sciences, Harvard University, 20 Oxford St., Cambridge, MA 02138, United States*

Received 20 April 2004; received in revised form 1 October 2004; accepted 13 October 2004

Editor: E. Boyle

Abstract

We examine the link between organic matter degradation, anaerobic methane oxidation (AMO), and sulfate depletion and explore how these processes potentially influence dolomitization. We determined rates and depths of AMO and dolomite formation for a variety of organic-rich sites along the west African Margin using data from Ocean Drilling Program (ODP) Leg 175. Rates of AMO are calculated from the diffusive fluxes of CH_4 and SO_4, and rates of dolomite formation are calculated from the diffusive flux of Mg. We find that the rates of dolomite formation are relatively constant regardless of the depth at which it is forming, indicating that the diffusive fluxes of Mg and Ca are not limiting. Based upon the calculated log IAP values, log K_{sp} values for dolomite were found to narrowly range between −16.1 and −16.4. Dolomite formation is controlled in part by competition between AMO and methanogenesis, which controls the speciation of dissolved CO_2. AMO increases the concentration of CO_3^{2-} through sulfate reduction, favoring dolomite formation, while methanogenesis increases the pCO_2 of the pore waters, inhibiting dolomite formation. By regulating the pCO_2 and alkalinity, methanogenesis and AMO can regulate the formation of dolomite in organic-rich marine sediments. In addition to providing a mechanistic link between AMO and dolomite formation, our findings provide a method by which the stability constant of dolomite can be calculated in modern sediments and allow prediction of regions and depth domains in which dolomite may be forming.

Keywords: anaerobic methane oxidation; dolomite; diagenesis

* Corresponding author. Current address: University of Delaware, Graduate College of Marine Studies, Cannon Lab 138, 700 Pilottown Rd., Lewes, Delaware 19958, United States. Fax: +1 302 645 4007.

E-mail addresses: tsmoore@bu.edu (T.S. Moore), rickm@bu.edu (R.W. Murray), kurtz@bu.edu (A.C. Kurtz), schrag@eps.harvard.edu (D.P. Schrag).

[1] Tel.: +1 617 353 36532; fax: +1 617 353 3290.

[2] Tel.: +1 617 358 2570; fax: +1 617 353 3290.

[3] Tel.: +1 617 495 7676; fax: +1 617 496 4387.

0012-821X/$ - see front matter © 2004 Elsevier B.V. All rights reserved.
doi:10.1016/j.epsl.2004.10.015

1. Introduction

With continued international concern over global hydrocarbon resources, increasing levels of study are being directed at the production and fate of methane (CH_4) in marine environments. One facet of this research has been to examine the role that upwardly diffusing CH_4 in many sedimentary sequences plays in the carbon cycle. Anaerobic methane oxidation (AMO), which is the oxidation of CH_4 to CO_2 using SO_4^{2-} as the terminal electron acceptor, has been found to coincide with the sulfate–methane transition (SMT) zone in many regions ([1–15]; and others). AMO is thought to convert a large fraction of the globally produced CH_4 to CO_2 [16] and has been linked to the formation of carbonate minerals [8,17–20].

AMO is mediated by a consortium of bacteria and archea [21–25]. This process occurs through the net reaction

$$CH_4 + SO_4^{2-} \rightarrow HCO_3^- + HS^- + H_2O \quad (1)$$

[3], where CH_4 and SO_4 are consumed in a 1:1 molar ratio. Areas in which AMO is occurring, such as organic-rich sediments along continental shelves, are characterized by a distinct SMT [3,5,16], an increase in carbonate alkalinity, a variety of different types of methane profiles [1–4,26,27], and a distinctive pattern of $\delta^{13}C$ in dissolved inorganic carbon (DIC). The $\delta^{13}C$ pattern is brought about by methanogenesis beneath the SMT according to

$$2CH_2O \rightarrow CH_4 + CO_2 \quad (2)$$

which produces isotopically heavy CO_2 and light CH_4 [4,28]. This results in heavier $\delta^{13}C$ pore water values at depth and lighter values in the SMT due to oxidation of the isotopically light CH_4 (Eq. (1)). Values of $\delta^{13}C$ in CH_4 commonly range between −50‰ and −110‰ [28].

In addition to its potential importance to the carbon cycle, AMO may play a critical role in the formation of dolomite in marine sediments. Although dolomite is one of the most abundant carbonate minerals, the method of its formation remains elusive, and the "Dolomite Problem" continues to be of wide interest. Under normal seawater conditions, dolomite is the most oversaturated carbonate mineral (e.g., [29]), and many pore waters are commonly supersaturated with respect to it (e.g., [30]). Although a major constituent of ancient sedimentary rocks, dolomite was only recently found in modern sediments [30–32]; and references therein).

Dolomite formed in relation to organic-rich marine sediments has been termed organogenic dolomite [30]. This type of dolomite is thought to be directly related to the diagenetic processes of sulfate reduction, methane oxidation, and methanogenesis ([32]; and references therein), as described further below, and is also controlled by the sources and sinks of dissolved Ca, Mg, and carbonate ions. Dissolution of existing primary calcite can provide a source of Ca [30,31,33]. Addition of Mg from subsurface advection and release from clays and other sources has been proposed, but, for most marine dolomites, these are considered to be minor sources [31]. Pore water depth profiles from the Deep Sea Drilling Project (DSDP) and Ocean Drilling Program (ODP) often show a gradual decrease in Mg

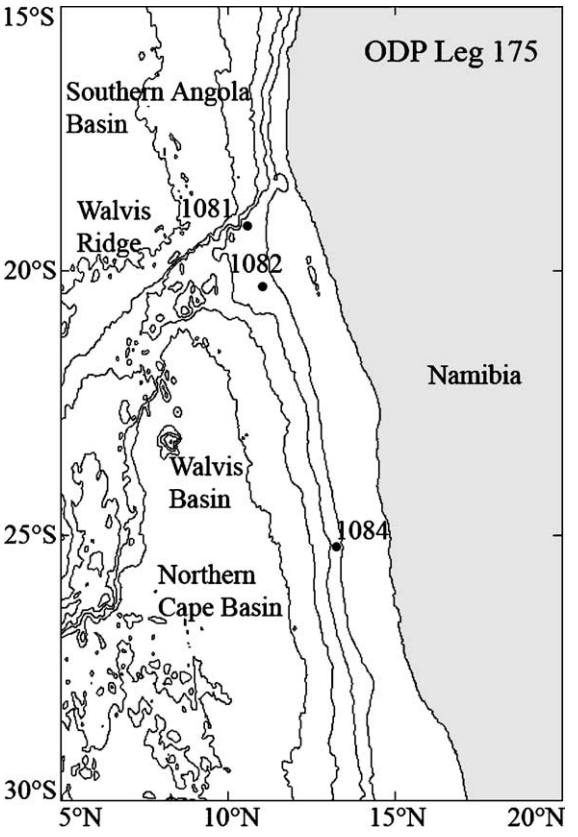

Fig. 1. Location of Sites 1075–1087 occupied during ODP Leg 175 [4151].

concentration, which is attributed to downward diffusion from seawater and formation of dolomite at depth (e.g., [30,31]). This implies that dolomite has to occur while the sediments are at relatively shallow subbottom depths for there to be a significant diffusive flux of Mg.

Potential sources of carbonate ion for dolomite formation include the dissolution of calcite, diffusion from seawater, AMO (Eq. (1)), and methanogenesis (Eq. (2)). The first two of these processes are relatively straightforward to assess, while the linkage between AMO, methanogenesis, and the potential inhibition of dolomitization by sulfate or Mg complexation remains unknown [32,34,35]. Because Mg and Ca can form complexed ions with sulfate, along with phosphate and carbonate, a lower effective concentration may result, which would inhibit dolomite formation. Furthermore, Lippman [37] found that hydration of these ions is relatively strong, especially in low concentrations of CO_3^{2-}, and Pytkowicz and Hawley [38] found that 11% of Mg and Ca in seawater are either hydrated or complexed ions. Arvidson and Mackenzie [39,40] have found that, while the interpolated rate at which dolomite forms at ambient temperatures is very slow, it is influenced by the carbonate alkalinity. An additional complication in accurately describing the environments and methods by which dolomite forms is that the thermodynamics of the system are poorly constrained. The calculated solubility product of dolomite varies by over two orders of magnitude [41,42], and so it is difficult to accurately predict when a solution is saturated with respect to dolomite.

We address these issues using an extensive pore water and sedimentary data set [43] gathered during ODP Leg 175 along the west African Margin (Fig. 1). In this region, many previous workers have documented the occurrence of AMO [11,15,44], and diagenetic dolomite occurring both as dispersed rhombs and as discrete layers up to several tens of

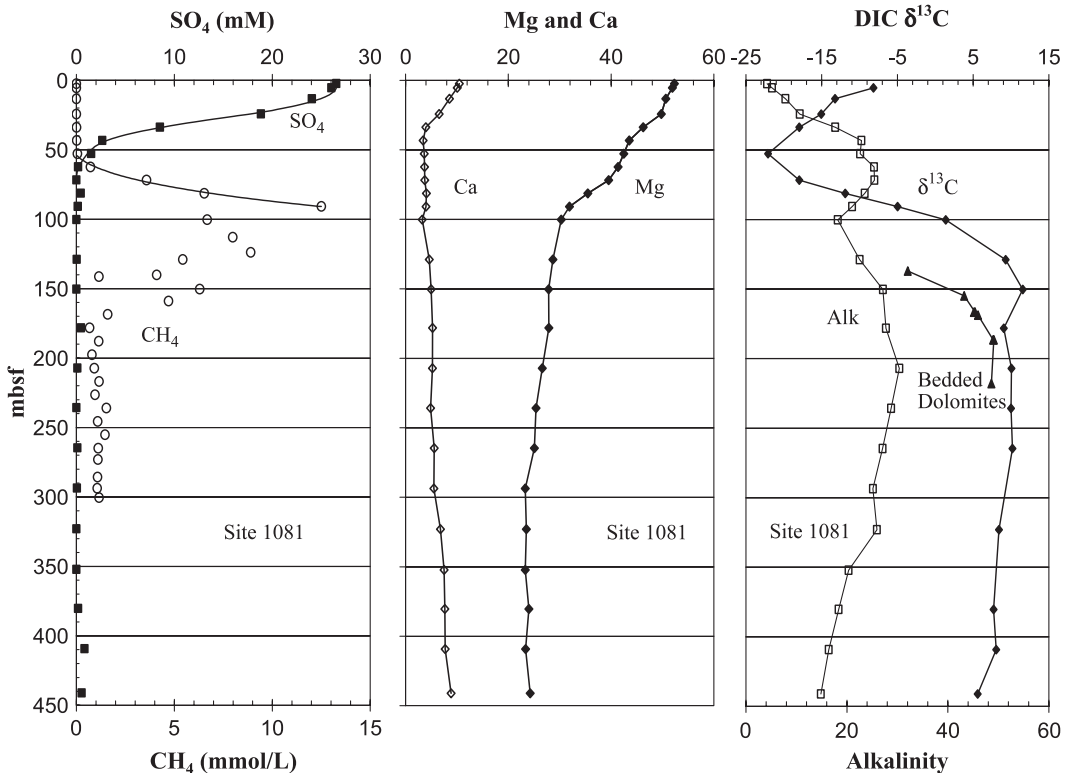

Fig. 2. Pore water profiles for ODP Site 1081. Measured $\delta^{13}C$ of the pore water are represented by ♦, and $\delta^{13}C$ of dolomite beds [47] are represented by ▲. Concentrations are in mM for sulfate, alkalinity, Ca, and Mg, mmol/L for methane, and ‰ PDB for $\delta^{13}C$.

centimeters thick have also been recovered ([45]; Fig. 2). As such, the data set is ideal to explore the relationship between AMO, sulfate inhibition, methanogenesis, and other parameters and to machinate on their potential effects on dolomite formation.

2. Site description and analytical methods

ODP Leg 175 occupied 13 sites off the coast of west Africa between 5°S and 32°S, with the goal of reconstructing the upwelling history of the Benguela current. This area is one of the largest regions of upwelling in the world and is characterized by organic-rich sediments and high sedimentation rates [45]. Sites were selected to cover a variety of geographic and depositional settings, including the Congo River fan, the Angola Dome, Walvis Ridge, and sites south of Walvis Ridge associated with intense upwelling (Fig. 1). Recovered sediments were primarily composed of diatomaceous and carbonate-rich clays [45]. We examine Sites 1081, 1082, and 1084 based upon their sampling resolution near the SMT and throughout the depth of the recovered material, the amount of dolomite observed, and shore-based analyses.

Sediment, pore water, and headspace CH_4 were analyzed aboard the JOIDES Resolution according to standard ODP procedures, and the methods and data may be found in Wefer et al. [45]. Shore-based analyses of $\delta^{13}C$ were conducted for organic carbon [46], dolomite [47], and dissolved inorganic carbon (DIC). For $\delta^{13}C$ measurements of DIC, samples were acidified with orthophosphoric acid, and the

Table 1
ODP Leg 175 DIC $\delta^{13}C$ (‰ PDB)

Site 1081		Site 1082				Site 1084	
Depth (mbsf)	$\delta^{13}C$	Depth (mbsf)	$\delta^{13}C$	Depth (mbsf)	$\delta^{13}C$	Depth (mbsf)	$\delta^{13}C$
5.40	−8.16	1.40	−2.23	43.15	3.39	1.40	−4.99
13.30	−13.23	2.90	−4.02	44.55	4.04	5.90	−9.10
24.30	−15.06	4.40	−7.27	47.05	4.94	10.40	−3.68
33.80	−17.95	7.53	−13.06	48.45	8.12	16.90	1.68
52.80	−22.09	9.20	−14.47	49.85	6.51	26.40	5.99
71.80	−17.96	10.70	−16.24	51.35	7.60	35.80	8.91
81.30	−11.89	12.10	−16.18	52.75	6.16	45.20	10.16
90.80	−4.97	13.50	−18.07	59.65	8.57	64.30	12.23
100.30	1.38	14.90	−17.85	78.45	10.59	73.80	13.61
128.94	9.29	16.25	−19.03	88.39	10.91	86.40	14.59
150.35	11.56	18.55	−20.46	97.50	12.22	93.07	13.86
178.20	9.05	19.95	−19.91	107.04	13.01	101.16	14.94
207.20	10.07	21.35	−19.17	131.07	13.88	130.90	16.05
235.80	9.99	22.75	−13.43	160.10	13.28	155.40	13.98
264.75	10.20	25.55	−9.42	189.77	13.04	193.88	12.74
323.00	8.40	28.05	−5.63	219.61	12.56	221.50	12.33
380.38	7.70	29.45	−3.60	248.75	12.35	253.30	12.15
409.28	8.04	30.85	−5.43	277.65	11.78	281.64	12.15
441.15	5.60	32.25	−2.35	306.49	11.41	310.91	12.45
		33.65	−1.50	334.04	11.20	340.00	12.16
		35.05	1.96	365.04	10.32	368.80	11.42
		37.55	1.17	392.34	9.89	397.70	11.39
		38.95	1.96	420.55	8.74	427.05	13.71
		40.35	2.34	461.61	6.72	457.10	10.69
		41.75	2.67	489.05	5.95	483.19	9.92
						540.60	8.39
						571.30	7.44
						599.90	6.11

evolved CO_2 measured on an Optimal gas-source mass spectrometer. Precision of the $\delta^{13}C$ measurements of DIC is ±0.1‰, and the data are provided in Table 1.

3. Approach

3.1. Diffusive fluxes

We calculate pore water fluxes by applying Fick's first law of diffusion

$$J_i = -\phi D_i \frac{\partial Ci}{\partial z} \quad (3)$$

where J_i is the flux of species i, ϕ is the porosity, D_i is the diffusivity in sediment of species i, C_i is the concentration of species i, and z is depth from sediment–water interface (increasing downward). Steady-state conditions $\left(\frac{\partial C_i}{\partial t} = 0\right)$ are assumed.

For purposes of this study, we will assume that the flux due to advection is slow relative to the diffusive term and can therefore be ignored, which is a common approach in studies of this kind [48–50]. Fluxes of Mg and Ca were calculated from Eq. (3). Fluxes of SO_4 and CH_4 were calculated based upon measured pore water profiles using the PROFILE model [49]. The PROFILE model is a profile interpretation method and has been used to calculate the diffusive flux of SO_4^{2-} in nearby sediments [11].

Values of D_i were calculated according to Iversen and Jørgensen [51]

$$D_i = \frac{D}{1 + 3(1-\phi)} \quad (4)$$

using the values of D provided in Table 2.

Table 2
Diffusion coefficients (D)[a,b]

[c]SO_4	2.08×10^{-2}
[c]CH_4	3.31×10^{-2}
[d]Mg	1.26×10^{-2}
[d]Ca	1.36×10^{-2}
[d]HCO_3	1.94×10^{-2}

[a] Units are m^2 $year^{-1}$.
[b] Calculated at 4 °C and average porosity for the sites.
[c] From Iversen et al. [51].
[d] From Atkins [66].

3.2. Anaerobic methane oxidation

As mentioned above, the presence of AMO can be recognized in pore water profiles by a distinct SMT and a subsequent decrease in DIC $\delta^{13}C$ and increase in alkalinity. Based upon Eq. (1), the flux of SO_4 and CH_4 into the SMT should be equal:

$$J_{SO_4} - J_{CH_4} = 0. \quad (5)$$

If SO_4 and CH_4 are being consumed in a 1:1 molar ratio (i.e., if they both have the same flux into the SMT), then it is reasonable to conclude that AMO is occurring, as has been the case in many similar studies of the west African Margin [11,15,44].

To quantify the contribution of AMO to pore water DIC (Eq. (1)), and therefore alkalinity, we employ an isotope mass balance [16,52] as follows:

$$\%CO_{2(CH_4)} = \frac{\delta^{13}C_{min} - \delta^{13}C_{bkg}}{\delta^{13}C_{CH_4} - \delta^{13}C_{bkg}} * 100, \quad (6)$$

where $\%CO_{2(CH_4)}$ is the percent of the $\sum CO_2$ that is derived from methane oxidation, $\delta^{13}C_{min}$ is the minimum value of DIC $\delta^{13}C$ observed at the SMT, $\delta^{13}C_{bkg}$ is the background DIC $\delta^{13}C$ value (0‰ to 4‰; [16]), and $\delta^{13}C_{CH_4}$ is the $\delta^{13}C$ of methane (−50‰ to −110‰; [28]).

3.3. Dolomite formation and calcite dissolution

As the exact pathway by which dolomite forms in organic-rich marine sediments is still unknown, we base our discussion upon the general equation

$$Ca^{2+} + Mg^{2+} + 2CO_3^{2-} \leftrightarrow CaMg(CO_3)_{2(\delta)}. \quad (7)$$

This does not take into account the effects of complexed ions and pH (e.g., [36]), but it is sufficient to describe the process of dolomite formation in a general sense. Assuming that the effects of uptake/release of Mg^{2+} from clay are minimal [31,34,53], then the rate of dolomite precipitation is equal to J^{Mg} (the diffusive flux of Mg). Assuming that stoichiometric dolomite is being formed, the rate of Ca taken up into dolomite, $J^{Ca}_{Dolomite}$ will equal the rate of Mg consumption. However, the Ca^{2+} concentration of the

pore water reflects both dolomite precipitation and calcite dissolution/precipitation, so the combination of Ca^{2+} and Mg^{2+} data can be used to quantify the rates of precipitation and/or dissolution of both carbonate minerals.

3.4. Quantification of uncertainty

To assess the validity of our approach, we quantified the uncertainty introduced by the assumptions described above. One source of uncertainty present in each flux calculation (regardless of species) arises from the assumption that the effect of advection caused by sediment compaction is minor. Lerman [54] noted that changes similar to what is observed here will result in an uncertainty of ~10%. Uncertainty in our analytical methods (e.g., measurements of SO_4^{2-}) is much less than that in our other calculations and can therefore safely be ignored. Uncertainty introduced by use of the PROFILE program [49] was tested by varying the physical parameters of the model (boundary conditions, etc.) and was found to be less than 10%. Uncertainty in 4 J_{CH} is similar to that of J_{SO_4} but is less precise due to the sampling methods employed by the ODP. Uncertainty in J_{Mg}, J_{Ca} and the rate of dolomite formation come largely from three sources [29–31,34,39]: the assumption that Mg is supplied only by seawater, the uptake/release of Mg and Ca from clays, and the assumption that stoichiometric dolomite is being formed. Based upon representative calculations, the uncertainty in these processes is approximately a factor of two.

Overall, uncertainties of the scale described here are common in pore water studies (e.g., [10,54,55]) as the processes targeted by these studies can be successfully addressed by even order-of-magnitude constraints. For example, published time scales in which "dolomite precipitation" occurs are dim at best and range from thousands to millions of years [56,57] at surface conditions and, to our knowledge, have yet to be more precisely constrained.

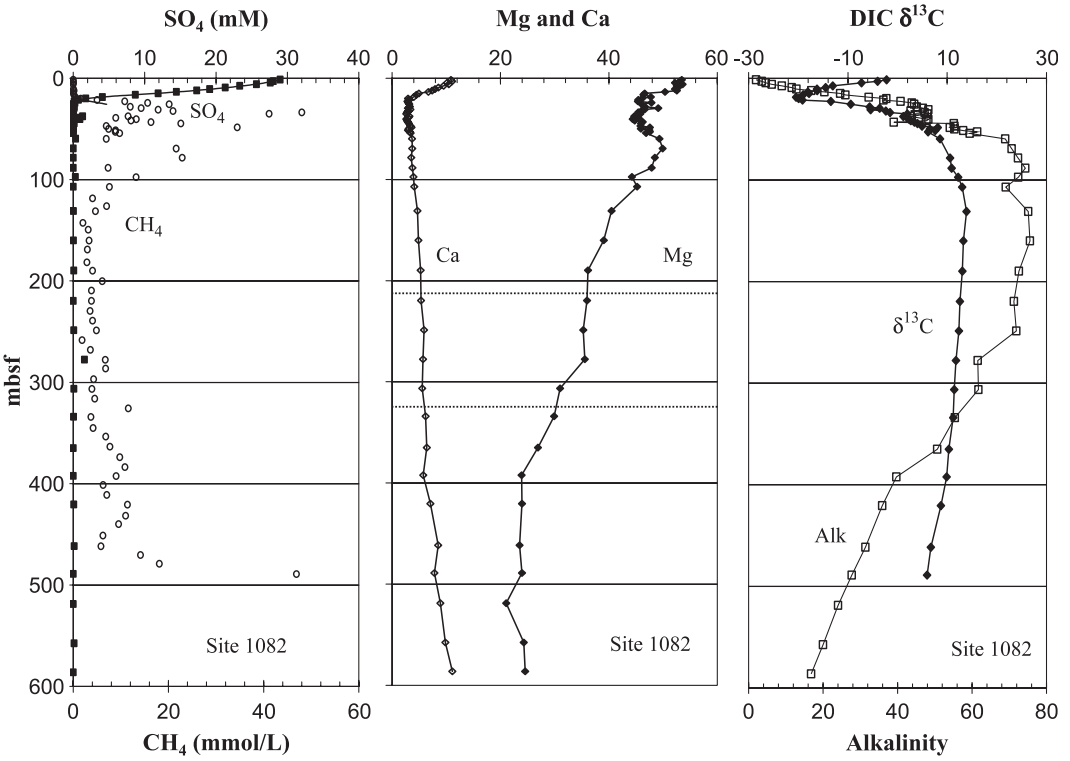

Fig. 3. Pore water profiles for ODP Site 1082. Concentrations are as in Fig. 2. Dashed lines indicate the location of dolomite beds [47].

4. Results

Site 1081 is characterized by having the highest amount of dispersed and bedded dolomite observed in these three sites (Fig. 2), the lowest alkalinity (Fig. 2), and the lowest sedimentation rate (40–150 m/my). Site 1082 is characterized by having intermediate values of alkalinity (Fig. 3) and sedimentation rate (70–200 m/my). Additionally, this site has less observed dolomite than Site 1081. Site 1084 has the highest measured alkalinity (Fig. 4), highest sedimentation rates (100–270 m/my), and has only one observed bedded dolomite layer. The occurrence of dispersed dolomite can be found in [45], and the locations of bedded dolomites are from Pufal and Wefer [47]. Additionally, Site 1084 has the second highest recorded alkalinity and NH4 recovered by the DSDP or ODP [43], exceeded only by Site 688 along the Peru Margin [58] and, as shown below, behaves significantly different from the other sites.

4.1. Occurrence of anaerobic methane oxidation

4.1.1. Site 1081

Pore water profiles at Site 1081 exhibit the characteristic pattern describing the occurrence of AMO ([9–13,15,44,49]; and others). At a depth range between 50 and 70 mbsf, there is a distinct transition between sulfate and methane (Fig. 2). Above this depth, the sulfate profile is nearly linear, indicating that there is diffusion with negligible consumption, and therefore the breakdown of organic matter by sulfate reduction is only of minor importance [13,48]. Below the SMT, the methane profile is also nearly linear for 20 m and then becomes more irregular with depth, which most likely represents methane loss during the ODP sampling process (e.g., [59]).

The DIC $\delta^{13}C$ minimum at the SMT (−22.09‰ PDB, Fig. 2) is slightly more negative than that of the $\delta^{13}C$ of the total organic carbon (TOC) found at this site (~−21‰ PDB, [46]). If only the degradation of

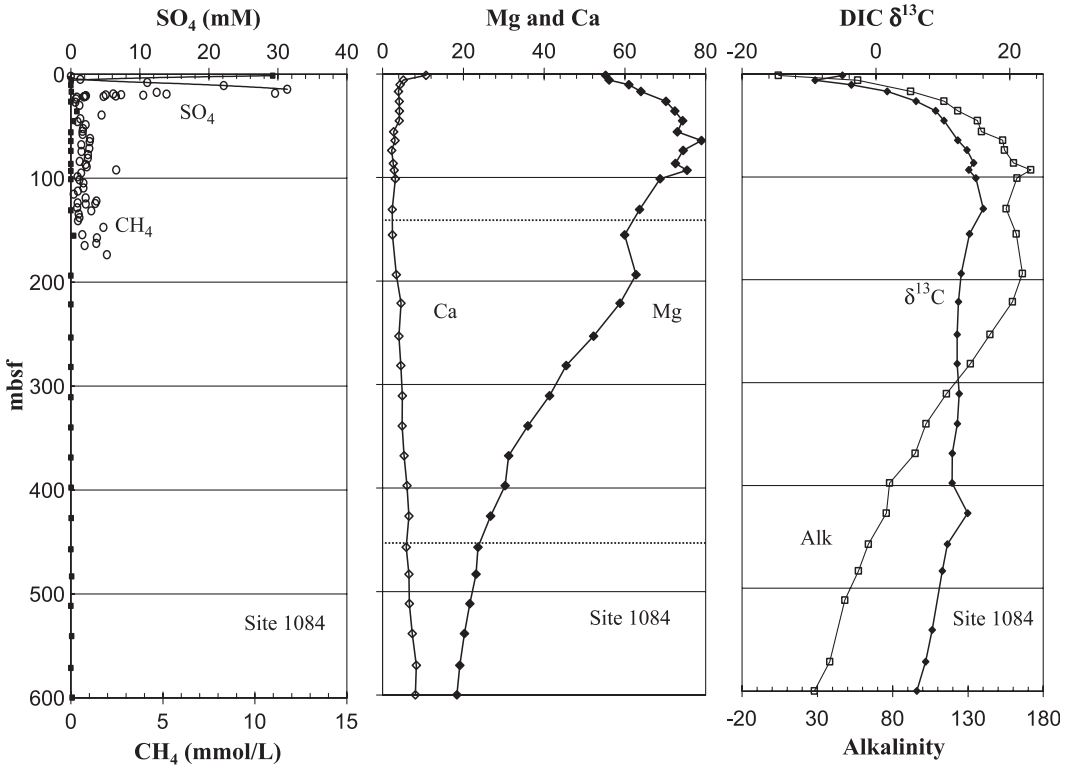

Fig. 4. Pore water profiles for ODP Site 1084. Concentrations are as in Fig. 2. Dashed lines indicate the location of dolomite beds [47].

organic matter were occurring through this depth range, then the $\delta^{13}C$ values of the DIC in pore water should have a value between that of seawater (0‰ PDB, [60]) and this organic matter. Thus, the isotope signature indicates the addition of an additional source of light carbon. The most likely source is AMO, which produces $\delta^{13}C$ values that are isotopically lighter than that predicted from simple mixing of the carbon derived from the degradation of organic matter and seawater, consistent with the observed values.

In the region above the SMT, the DIC $\delta^{13}C$ profile is concave downward and approaches 0‰ PDB at the sediment water interface. Below the SMT, the DIC $\delta^{13}C$ profile is also concave downward and reaches a maximum of +11.56‰ PDB at 150 mbsf. These large positive values result from methanogenesis below the SMT due to the preferential uptake of ^{12}C into methane and partitioning of ^{13}C into CO_2 [61]. Additionally, alkalinity increases at the SMT (Fig. 2), consistent with the production of either/or HCO_3^-, CO_3^{2-}, and HS^- during AMO (Eq. (1)).

The flux of sulfate and methane into the SMT can be used to calculate the rate of AMO ([9–11,13,15,44,50]; and others). Using the PROFILE model [49] to calculate the flux of SO_4 and CH_4 into the SMT (Fig. 2), we obtain a flux of -2.8×10^{-4} mM m^{-2} $year^{-1}$ for SO_4 and -2.1×10^{-4} mmol/L m^{-2} $year^{-1}$ for CH_4. These two values are in approximate balance, particularly considering the large uncertainty in the ODP CH_4 measurements. Using the isotopic mass balance (Eq. (6); [16,52]) gives an AMO contribution of 31% to the total carbonate alkalinity at the SMT. These results are comparable to those of Zabel and Schulz [15] who found that AMO contributed ~30% of the $\sum CO_2$ in the same region.

4.1.2. Site 1082

Site 1082 exhibits the characteristic pore water profile of a distinct SMT and a subsequent decrease in $\delta^{13}C$ (Fig. 3). The SMT occurs between 18–24 mbsf and has a nearly linear SO_4 profile, indicating, as at Site 1081, that the breakdown of organic matter by sulfate reduction is minor [13,48]. However, unlike Site 1081, alkalinity does not peak at the SMT, although there is a noticeable change in the profile at that depth. Alkalinity continues to increase with depth below the SMT, indicating that there is another source, most likely related to CH_4 production (Eq. (2)), as can be seen by the increase in $\delta^{13}C$ values. The rate of SO_4 consumption is -3.9×10^{-3} mM m^{-2} $year^{-1}$, and the rate of CH_4 consumption is -5.8×10^{-3} mmol m^{-2} $year^{-1}$. The contribution of AMO to the total alkalinity from the isotope mass balance calculation (Eq. (6)) is 29%.

4.1.3. Site 1084

At Site 1084, the SMT is located at the very shallow depth of 6 mbsf, with a subsequent decrease in $\delta^{13}C$ (Fig. 4). The characteristic increase in alkalinity is not seen at this specific depth most likely due to high rates of methanogenesis at depth. As at Site 1082, alkalinity continues to increase with depth below the SMT, indicating that there is another source, most likely related to CH_4 production (Eq. (2)), as can be seen in the $\delta^{13}C$ profile (Fig 4). The rate of SO_4 consumption is -1.6×10^{-2} mmol m^{-2} $year^{-1}$, while the rate of CH_4 consumption is -6.7×10^{-3} mmol m^{-2} $year^{-1}$. These results agree within 41%, and the difference between them is most likely an artifact of CH_4 degassing. The contribution of AMO to the total alkalinity from the isotope mass balance calculation (Eq. (6)) is only 12%, indicating that the upward diffusive flux of CO_2 produced during methanogenesis dominates the pore water alkalinity.

4.2. Mg and Ca pore water fluxes

Considering all sites together, the diffusive fluxes of Mg and Ca can provide insight into the rates of calcite

Table 3
Calculated diffusive fluxes[a]

	Depth (mbsf)	J^{Mg}	Depth (mbsf)	J^{Ca}
Site 1081	2.4–100	1.1×10^{-3}	2.4–35	1.2×10^{-3}
	100–260	1.3×10^{-4}	35–441	-5.4×10^{-5}
	260–441	7.6×10^{-6}		
Site 1082	1.4–20	3.4×10^{-2}	1.4–20	2.8×10^{-3}
	20–45	2.8×10^{-4}	20–586	-5.7×10^{-5}
	45–70	-8.6×10^{-4}		
	70–130	8.8×10^{-4}		
	130–390	3.0×10^{-4}		
	390–586	-1.3×10^{-6}		
Site 1084	1.4–65	-2.2×10^{-3}	1.4–10	5.7×10^{-3}
	65–370	7.2×10^{-4}	10–600	-5.6×10^{-5}
	370–600	1.8×10^{-4}		

[a] mM m^{-2} $year^{-1}$.

dissolution and dolomite precipitation and the depth domains in which they are occurring. Diffusive fluxes were calculated using Eq. (3) and are listed in Table 3. All three sites have the same basic pore water trends with depth. Dissolved Ca^{2+} initially decreases to a minimum of ~3 mmol/L. Dissolved Mg^{2+} decreases with depth, and the rate at which it decreases changes abruptly at depth. Site 1081 demonstrates this most clearly, while Sites 1082 and 1084 have more variability in the upper sediments.

5. Discussion

5.1. Anaerobic methane oxidation, methanogenesis, and $\sum DIC$

Rates of AMO observed here agree well with other observed rates on the west African Margin [15] and the Black Sea [13]. The rate of AMO and the depth of the SMT appear to be directly related, where Site 1081 has the lowest rate of AMO with a deeper SMT and Site 1084 has the highest rate of AMO with the shallowest SMT. Furthermore, the rate of AMO is positively correlated with sedimentation rate. This could be due in part to enhanced organic matter preservation, especially of the more labile fraction, at higher sedimentation rates, which could then result in higher rates of methanogenesis. The potential effect of differences in grain size and other parameters perhaps critical to the degradation of organic matter [62–65] cannot be examined given the available data set but may also be important.

Since the amount of SO_4 supplied by seawater from above the SMT is diffusion-limited, CH_4 production and diffusion will control the rate of AMO and the depth of the SMT. From Eq. (3), the flux of a species can be increased by either making the change in concentration greater (∂C) or making the change in depth smaller (∂z). From Eq. (5), J_{CH_4} and J_{SO_4} at the SMT should be equal, and therefore, as the rate of methanogenesis increases, J_{CH_4} will also increase, which will result in a higher rate of AMO. To increase J_{SO_4}, the depth of the SMT must be shallower (closer to the seawater source). This trend can be verified by the increase in alkalinity and rates of AMO and depth of the SMT between Sites 1081, 1082, and 1083 (Figs. 2–4; Table 2).

5.2. Dolomitization: competition between AMO and methanogenesis

The trends between these three sites are also reflected in the amount of dolomite observed, although it is counterintuitive to what would be expected were the total alkalinity is the main controlling feature of dolomitization. Recall that Site 1081 has the lowest total alkalinity of the three sites yet the most abundant dolomite, and Site 1084 has the extremely high total alkalinity yet minimal dolomite. As the formation of dolomite is dependent in part upon the concentration of CO_3^{2-} (Eq. (7)), it is the speciation of dissolved carbonate in the system, not the total alkalinity, which directly affects the formation of dolomite. Both AMO and methanogenesis increase the pCO_2, which shifts the carbonate equilibria towards H_2CO_3 and lowers the carbonate saturation state. However, AMO also increases the alkalinity, which will increase CO_3^{2-}, more than compensating for the increase in pCO_2. Depths where the alkalinity is dominated by AMO should favor dolomite formation, while depths dominated by methanogenesis should not. Hence, the speciation of $\sum CO_2$ associated with AMO and methanogenesis is controlled by the relative rates of AMO and methanogenesis. Based upon this, the carbon isotope mass balance (Eq. (6)) can be used to determine the contribution of AMO to $\sum CO_2$ and thereby predict at which sites the formation of CO_3^{2-} and dolomite are favored.

Depths where dolomite is forming at present can be identified where there are significant sinks in the dissolved Mg profile. We predict that dolomite should be forming below 100 mbsf at Site 1081, between 20–70 mbsf and below 390 mbsf at Site 1082, and below

Table 4
Calculated rates of dolomite formation[a,b]

	Depth (mbsf)	Rate of formation
Site 1081	100–260	1.3×10^{-4}
	260–441	7.6×10^{-6}
Site 1082	20–45	2.8×10^{-4}
	70–390	3.0×10^{-4}
Site 1084	370–600	1.8×10^{-4}

[a] mM m^{-2} yr^{-1}.
[b] See Eq. 7.

~400 mbsf at Site 1084. Calculated rates of dolomite formation are equal to the flux of Mg^{2+} into these areas and are listed in Table 4. The amount of Ca^{2+} taken up during dolomite formation is equal to the amount of Mg (Eq. (7)). Dissolved Ca at all three sites reach a minimum of ~3 mM at a relatively shallow depth followed by a gradual increase with depth. At Site 1081, the fluxes of Ca and Mg are initially similar until Ca reaches a minimum at 35 mbsf. Below this, Mg continues to decrease, while Ca remains relatively constant. This suggests the formation of an authigenic Ca-bearing mineral phase near the SMT, such as that seen by Zabel and Schulz [15] in the Congo Fan, and that the pore waters are in equilibrium with a Ca-bearing mineral phase below this depth. The profiles clearly indicate that the Mg depletion is deeper, indicating that Ca is not limiting the formation of dolomite and that the dissolution of the Ca-bearing phase between 35 mbsf and the deep Mg sink is providing the additional Ca necessary for dolomitization at depth. The same trend is seen in Sites 1082 and 1084. This is dolomitization as calcite is dissolving and being replaced at depth by dolomite. Using a log K_{sp} of −8.48 for calcite (25 °C, 1 atm; [28]), the pore water $[CO_3^{2-}]$ can then be calculated for any pore waters where the sediments are in equilibrium with calcite (i.e., where the dissolved Ca concentration remains relatively constant) by

$$[CO_3^{2-}] = \frac{K_{spCalcite}}{[Ca^{2+}]}. \quad (8)$$

Once the CO_3^{2-} concentration of the pore waters has been determined, the ion activity product IAP of dolomite can be calculated by

$$IAP_{Dolomite} = [Ca][Mg][CO_3]^2. \quad (9)$$

Assuming that concentration is equal to activity, the measured [Mg] and [Ca] and the calculated $[CO_3]$ can be substituted into Eq. (9), and the log IAP can then be found for all depths at which calcite is

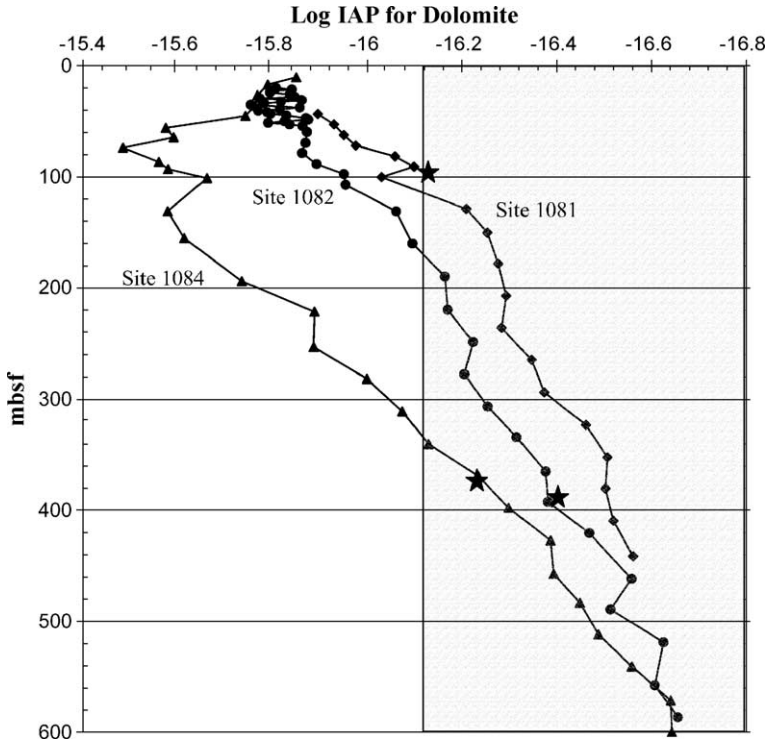

Fig. 5. Calculated log IAP values for dolomite in ODP Sites 1081, 1082, and 1083. Grey area indicates depths at which the log IAP of dolomite is greater than 16.1. Stars indicate depths of predicted dolomite formation based upon the dissolved Mg profiles.

dissolving. Although our IAP calculations neglect the effects of temperature and pressure on the equilibrium constant of calcite, this will introduce much less uncertainty than the assumption of equilibrium with calcite. Comparing the log IAP values (Fig. 5) to areas in which dolomite is predicted to be forming (Table 3) reveals that, at all three locations, dolomite is forming at a log IAP of −16.1 to −16.2 or lower. If dolomite is precipitating when the IAP of the pore waters is equal to or lesser than the K_{sp} of dolomite, then the log K_{sp} for dolomite in these sites will then be equal to the log IAP (−16.1 to −16.4) at which dolomite initially begins to form. These values are more than an order of magnitude greater than the predicted range of log K for stoichiometric dolomite (log K=−17.33 to −19.71; [42]; and references therein) but agree extremely well with calculated log K values of disordered dolomite (log K=−16.52; [41]).

Stratigraphically above the SMT, the IAP of dolomite could not be calculated since the concentration of dissolved Ca is changing, and hence we cannot assume equilibrium with calcite. However, SO_4 is thought to inhibit dolomite formation [34,36], and its presence shallower than the SMT could therefore be preventing dolomite formation. At Site 1082, the decrease in [Mg] between 20–45 mbsf could be interpreted as indicating dolomite formation [43]. However, this is not supported by the calculated IAP values. We interpret the Mg decrease, therefore, as indicating nonsteady state conditions in this narrow depth range by a process which has not yet been identified. At Site 1084, the peak in dissolved Mg at 65 mbsf is most likely due to the dissolution of previously formed dolomite (such as in Site 1082) or of another Mg-bearing mineral phase. It is unlikely that complexation of Mg (e.g., by CO_3^{2-} or Cl^-) is responsible for the maximum at Site 1084 as the Mg values exceed seawater concentrations, and thus the maximum must be caused by addition from some other Mg source.

Further evidence for spatially and geochemically linking AMO and dolomite precipitation is demonstrated by the $\delta^{13}C$ values reported by Pufahl and Wefer [47] for the bedded dolomites in this region (Fig. 2). These values parallel the pore water $\delta^{13}C$ values at depth, with the lighter values seen in these beds, indicating that they had to have initially formed near 100 mbsf and that continual dolomite precipitation has been occurring.

6. Summary and conclusions

Pore water profiles from deep drilling sites visited during ODP Leg 175 along the west African Margin provide a good natural laboratory to study the formation of dolomite in modern organic-rich sediments. The three sites discussed here record a progression in methanogenesis and dolomitization. The depth at which SO_4 is depleted is related to alkalinity, and sites with high alkalinity typically have a shallow SMT. In general, dissolved Mg decreases with depth, and the pore water profile undergoes a noticeable change, which is attributed to dolomite formation. Dissolved Ca typically decreases with depth until it reaches a concentration of ~3 mM after which it gradually increases due to calcite dissolution.

Diffusive fluxes calculated from pore water profiles of dissolved SO_4 and CH_4 demonstrate that there is a correlation between sedimentation rate, the rate of AMO, and the depth of the SMT, with higher rates of methanogenesis causing higher rates of AMO and a shallow SMT. Additionally, sites with higher rates of AMO have less dolomite than those with lower rates of AMO. The rates of dolomite formation are relatively constant regardless of the depth at which it is forming, indicating that the diffusive fluxes of Mg and Ca are not limiting. Instead, the concentration of CO_3^{2-} appears to control the stability of dolomite based upon the calculated log IAP. Additionally, the formation of dolomite appears inhibited by the presence of SO_4 most likely due to the presence of Mg–SO_4 complexes.

The formation of dolomite in these sites is controlled by competition between AMO and methanogenesis on the speciation of dissolved pore water CO_2. Both AMO and methanogenesis increase the pCO_2, shifting the carbonate equilibria towards H_2CO_3 and lowering the carbonate saturation state. This increase in pCO_2 prohibits the formation of dolomite at the alkalinity maximum. However, the increase in alkalinity during AMO increases the CO_3^{2-} concentration, offsetting the increase in pCO_2, resulting in a net increase in CO_3^{2-}. By regulating the pCO_2 and alkalinity, methanogenesis and AMO control the formation of dolomite in organic-rich marine sediments. These findings allow us to calculate the stability constant

for dolomite in a modern environment. Additionally, they provide us with the methods to predict the formation of dolomite in modern organic-rich marine environments.

Acknowledgements

This work was supported by a JOI/USSSP grant to R.W. Murray as well as institutional support provided by Boston University. We thank G. Dickens and P. Berg for helpful comments throughout this project and M. Zabel and an anonymous reviewer for their comments on the manuscript. We thank Captain Methane for The Words.

References

[1] C.S. Martens, R.A. Berner, Methane production in the interstitial waters of sulfate-depleted marine sediments, Science 185 (1974) 1167–1169.
[2] R.O. Barnes, E.D. Goldberg, Methane production and consumption in anoxic marine sediments, Geology 4 (1976) 297–300.
[3] W.S. Reeburgh, Methane consumption in Cariaco Trench waters and sediments, Earth Planet. Sci. Lett. 28 (1976) 337–344.
[4] C.S. Martens, R.A. Berner, Interstitial water chemistry of anoxic Long Island Sound sediments: 1. Dissolved gases, Limnol. Oceanogr. 22 (1) (1977) 10–25.
[5] W.S. Reeburgh, Anaerobic methane oxidation: rate depth distributions in Skan Bay sediments, Earth Planet. Sci. Lett. 47 (1980) 345–352.
[6] F.J. Sansone, C.S. Martens, Methane production from acetate and associated methane fluxes from anoxic coastal sediments, Science 211 (1981) 707–709.
[7] N. Iversen, B.B. Jørgensen, Anaerobic methane oxidation rates at the sulfatemethane transition in marine sediments from Kattegat and Skagerrak (Denmark), Limnol. Oceanogr. 30 (5) (1985) 944–955.
[8] N.O. Jorgensen, Methane-derived carbonate cementation of marine sediments from the Kattegat, Denmark: geochemical and geological evidence, Mar. Geol. 103 (1992) 1–13.
[9] N.E. Blair, R.C. Aller, Anaerobic methane oxidation on the Amazon shelf, Geochim. Cosmochim. Acta 59 (18) (1995) 3707–3715.
[10] W.S. Borowski, C.K. Paull, W. Ussler III, Marine pore-water sulfate profiles indicate in situ methane flux from underlying gas hydrate, Geology 24 (7) (1996) 655–658.
[11] H. Fossing, T.G. Ferdelman, P. Berg, Sulfate reduction and methane oxidation in continental margin sediments influenced by irrigation (South-East Atlantic off Namibia), Geochim. Cosmochim. Acta 64 (5) (2000) 897–910.
[12] G.R. Dickens, Sulfate profiles and barium fronts in sediment on the Blake Ridge: present and past methane fluxes through a large gas hydrate reservoir, Geochim. Cosmochim. Acta 65 (4) (2001) 529–543.
[13] B.B. Jørgensen, A. Weber, J. Zopfi, Sulfate reduction and anaerobic methane oxidation in Black Sea sediments, Deep-Sea Research, Part 1. Oceanogr. Res. Pap. 48 (2001) 2097–2120.
[14] M.J. Whiticar, M.E. Elvert, Organic geochemistry of Saanich Inlet, BC, during the Holocene as revealed by Ocean Drilling Program Leg 169S, Mar. Geol. 174 (2001) 249–271.
[15] M. Zabel, H.D. Schulz, Importance of submarine lanslides for non-steady state conditions in pore water systems—lower Zaire (Congo) deep-sea fan, Mar. Geol. 176 (2001) 87–99.
[16] W.S. Reeburgh, A Major Sink and Flux Control for Methane in Marine Sediments: Anaerobic Consumption, University of Miami, Miami, FL, 1982.
[17] H. Irwin, C. Curtis, M. Coleman, Isotopic evidence for source of diagenetic carbonates formed during burial of organic-rich sediments, Nature 15 (1977) 209–213.
[18] C.S. Teal, S.J. Mazzullo, W.D. Bischoff, Dolomitization of holocene shallow-marine deposits mediated by sulfate reduction and methanogenesis in normal-salinity seawater, Northern Belize, J. Sediment. Res. 70 (3) (2000) 649–663.
[19] G. Aloisi, C. Pierre, J. Rouchy, J. Faugeres, Isotopic evidence of methane-related diagenesis in the mud volcanic sediments of the Barbados Accretionary Prism, Continent. Shelf Res. 22 (2002) 2355–2372.
[20] R. Luff, K. Wallmann, Fluid flow, methane fluxes, carbonate precipitation and biogeochemical turnover in gas hydrate-bearing sediments at Hydrate Ridge, Cascadia Margin: numerical modeling and mass balances, Geochim. Cosmochim. Acta 67 (18) (2003) 3403–3421.
[21] A. Boetius, K. Ravenschlag, C.J. Schubert, D. Rickert, F. Widdel, A. Gieseke, R. Amann, B.B. Jørgensen, U. Witte, O. Pfannkuche, A marine consortium apparently mediating anaerobic oxidation of methane, Nature 407 (2000) 623–626.
[22] V.J. Orphan, C.H. House, K. Hinrichs, K.D. McKeegan, E.F. DeLong, Methane-consuming archea revealed by directly coupled isotopic and phylogenic analysis, Science 293 (2001) 484–487.
[23] S. D'Hondt, S. Rutherford, A.J. Spivack, Metabolic activity of subsurface life in deep-sea sediments, Science 295 (2002) 2067–2070.
[24] D.L. Valentine, W.S. Reeburgh, New perspectives on anaerobid methane oxidation, Environm. Microbiol. 2 (5) (2000) 477–484.
[25] S.G. Wakeham, C.M. Lewis, E.C. Hopmans, S. Schouten, J.S. Sinninghe Damste, Archea mediate anaerobic oxidation of methane in deep euxinic waters of the Black Sea, Geochim. Cosmochim. Acta 67 (7) (2003) 1359–1374.
[26] W.S. Reeburgh, D.T. Heggie, Microbial methane consumption reactions and their effect on methane distributions in freshwater and marine environments, Limnol. Oceanogr. 22 (1) (1977) 1–9.
[27] C. Hensen, M. Zabel, K. Pfiefer, T. Schwenk, S. Kasten, N. Riedenger, H.D. Schulz, A. Boetius, Control of sulfate pore-water profiles by sedimentary events and the significance of

anaerobic oxidation of methane for the burial of sulfur in marine sediments, Geochim. Cosmochim. Acta 67 (14) (2003) 2631–2647.
[28] M.J. Whiticar, Carbon and hydrogen isotope systematics of bacterial formation and oxidation of methane, Chem. Geol. 161 (1999) 291–314.
[29] J.W. Morse, F.T. Mackenzie, Geochemistry of Sedimentary Carbonates, Elsevier, 1990.
[30] J.S. Compton, Degree of supersaturation and precipitation of organogenic dolomite, Geology 16 (1988) 318–321.
[31] P.A. Baker, S.J. Burns, Occurrence and formation of dolomite in organic-rich continental margin sediments, Am. Assoc. Pet. Geol. Bull. 69 (11) (1985) 1917–1930.
[32] S.J. Mazzullo, Organogenic Dolomitization in peritidal to deep-sea sediments, J. Sediment. Res. 70 (1) (2000) 10–23.
[33] K. Pfeifer, C. Hensen, M. Adler, F. Wenzhfer, B. Weber, D. Schulz, Modeling of subsurface calcite dissolution, including the respiration and reoxidation processes of marine sediments in the region of equatorial upwelling off Gabon, Geochim. Cosmochim. Acta 62 (4) (2002) 4247–4259.
[34] P.A. Baker, M. Kastner, Constraints on the formation of sedimentary dolomite, Science 213 (1981) 214–216.
[35] M. Kastner, Control of dolomite formation, Nature 311 (1984) 410–411.
[36] M. Slaguther, R.J. Hill, The influence of organic matter in organogenic dolomitization, J. Sediment. Petrol. 61 (2) (1991) 296–303.
[37] F. Lippmann, Sedimentary Carbonate Minerals, Springer-Verlag, Berlin, 1972.
[38] R.M. Pytkowicz, J.E. Hawley, Bicarbonate and carbonate ion-pairs and a model of seawater at 25 °C, Limnol. Oceanogr. 19 (1974) 223–232.
[39] R.S. Arvidson, F.T. Mackenzie, Tentative kinetic model for dolomite precipitation rate and its application to dolomite distribution, Aquat. Geochem. 2 (1997) 965–984.
[40] R.S. Arvidson, F.T. Mackenzie, The dolomite problem: control of precipitation kinetics by temperature and saturation state, Am. J. Sci. 299 (1999) 257–288.
[41] L.A. Hardie, Dolomitization: a critical view of some current views, J. Sediment. Petrol. 57 (1) (1987) 166–183.
[42] J.W. Morse, R.S. Arvidson, The dissolution kinetics of major sedimentary carbonate minerals, Earth-Sci. Rev. 58 (2002) 51–84.
[43] R.W. Murray, R. Wigley, Shipboard Scientific Party, 20. Interstitial water chemistry of deeply buried sediments from the Southwest African Margin: a preliminary synthesis of results from Leg 175, Proc. Ocean Drill. Prog. Init. Rept. 175 (1998) 547–553.
[44] C. Niewöhner, C. Hensen, S. Kasten, M. Zabel, H.D. Schulz, Deep sulfate reduction completely mediated by anaerobic methane oxidation in sediments of the upwelling region area off Nambia, Geochim. Cosmochim. Acta 62 (3) (1998) 455–464.
[45] G. Wefer, W.H. Berger, C. Richter, et al. Proceedings of the Ocean Drilling Program, Initial Reports, vol. 175, Ocean Drilling Program, College Station, TX, 1998.
[46] H. Lin, C. Lin, P.A. Meyers, Data report: carbonate, organic carbon, and opal concentrations and organic $\delta^{13}C$ values of sediments from sites 1075–1082 and 1084, Southwest Africa margin, Proc. Ocean Drill. Prog. Sci. Results 175 (2001) http://www-odp.tamu.edu/publications/175_SR/VOLUME/CHAPTERS/SR175_17.PDF.
[47] P.K. Pufahl, G. Wefer, Data report: petrographic, cathodoluminescent, and compositional characteristics of organogenic dolomites from the Southwest African margin, Proc. Ocean Drill. Prog. Sci. Results 175 (2001) http://www-odp.tamu.edu/publications/175_SR/VOLUME/CHAPTERS/SR175_17.PDF.
[48] R.A. Berner, Early Diagenesis, Princeton University Press, Princeton, NJ, 1980.
[49] P. Berg, N. Risgaard-Petersen, S. Rysgaard, Interpretation of measured concentration profiles in sediment pore water, Limnol. Oceanogr. 43 (7) (1998) 1500–1510.
[50] W.S. Borowski, T.M. Hoehler, M.J. Alperin, N.M. Rodriquez, C.K. Paull, Significance of anaerobic methane oxidation in methane-rich sediments overlying the Blake Ridge gas hydrates, Proc. Ocean Drill. Prog. Sci. Results 164 (2000) 87–99.
[51] N. Iversen, B.B. Jørgensen, Diffusion coefficients of sulfate and methane in marine sediments: influence of porosity, Geochim. Cosmochim. Acta 57 (1993) 571–578.
[52] D.J. Shultz, J.A. Calder, Organic carbon 13C/12C variations in estuarine sediments, Geochim. Cosmochim. Acta 40 (1976) 331–335.
[53] J.S. Compton, R. Siever, Diffusion and mass balance of Mg during early dolomite formation. Monterey Formation, Geochim. Cosmochim. Acta 50 (1986) 125–135.
[54] A. Lerman, 18. Migrational processes and chemical reaction in interstitial waters, Geochemical Processes in Water and Sediment Environments, Wiley Interscience, New York, 1979.
[55] C.M. Bethke, Geochemical Reaction Modeling, Oxford University Press, 1996.
[56] P.W. Choquette, R.P. Steinen, Mississippian non-supratidal dolomite, Ste. Genevieve Limestone, Illinois Basin: evidence for mixed-water dolomitization, in: D. Zenger, J. Dunham, R. Ethington (Eds.), Concepts and Models of Dolomitization, SEPM Spec. Publ., 28, 1980, pp. 163–196.
[57] S.O. Sears, F.J. Lucia, Dolomitization of northern Michigan Niagara reefs by brine refluxion and freshwater/seawater mixing, in: D. Zenger, J. Dunham, R. Ethington (Eds.), Concepts and Models of Dolomitization, SEPM Spec. Publ. 28, 1980, pp. 197–214.
[58] M. Kastner, H. Elderfield, J.B. Martin, E. Suess, K.A. Kvenvolden, R.E. Garrison, Diagenesis and Interstitial-Water Chemistry at the Peruvian Continental Margin—Major Constituents and Strontium Isotopes, Ocean Drilling Program, College Station, TX, 1990.
[59] G.R. Dickens, C.K. Paull, P. Wallace, ODP Leg 164 Scientific Party, Direct measurement of in situ methane quantities in a large gas hydrate reservoir, Nature 385 (1997) 426–428.

[60] W.S. Broecker, T.-H. Peng, Tracers in the Sea, Columbia University, Lamont-Doherty Geological Observatory, New York, 1982.
[61] J.F. Barker, P. Fritz, Carbon isotope fractionation during microbial methane oxidation, Nature 293 (1981) 289–291.
[62] R.G. Keil, E. Tsamakes, C.B. Fuh, C. Giddings, J.I. Hedges, Mineralogical and textural controls on the organic composition of coastal marine sediments: hydrodynamic separation using SPLITT-fractionation, Geochim. Cosmochim. Acta 58 (1994) 879–893.
[63] L.M. Mayer, Surface area control of organic carbon accumulation in continental shelf sediments, Geochim. Cosmochim. Acta 58 (1994) 1271–1284.
[64] J.I. Hedges, R.G. Keil, Sedimentary organic matter preservation: an assessment and speculative synthesis, Mar. Chem. 49 (1995) 81–115.
[65] B.D. Ransom, D. Kim, M. Kastner, S. Wainwright, Organic matter preservation on continental slopes: importance of mineralogy and surface area, Geochim. Cosmochim. Acta 62 (1998) 1329–1345.
[66] P.W. Atkins, Physical Chemistry, Oxford University Press, Oxford, 1978.